A model-based approach to video-based eye tracking

("Special Issue in Physiological Optics")

FENG LI, SUSAN KOLAKOWSKI and JEFF PELZ*

Chester F. Carlson Center for Imaging Science, Rochester Institute of Technology,
54 Lomb Memorial Drive, Rochester, NY 14623, USA

Video-based eye tracking typically relies on tracking the pupil and a first-surface corneal reflection (CR) of an illumination source. The positional difference between these two features is used to determine the observer's eye-in-head orientation. With the use of head-mounted eye trackers, this positional difference is unavoidably affected by relative movements between the eye tracking camera and the subject's eye. Video-based trackers also suffer from problems resulting in poor CR detection, such as spurious reflections being mistaken as the desired CR. We approach these problems by modelling how these features – pupil and CR – are affected by different relative movements of the eye. Optical relationships between the offset of the apparent pupil centre and that of the CR are derived. An experiment was conducted with five observers to support these derivations. Our solutions to the aforementioned problems using these offset relationships are provided. The first application compensates for movements of an eye tracking camera with respect to the eye and reduces noise in the final eye orientation data. The second application is prediction of CR locations for artefact removal in our new eye tracking system prototype.

Keywords: Video-based eye tracking; Translational eye movement; Rotational eye movement; Camera movement; Pupil; Corneal reflection

1. Introduction

Beginning as early as the nineteenth century, researchers have been eager to explore hidden mysteries behind the human visual system. Since then, many groundbreaking techniques for recording eye movements have been invented and applied in practise: in 1898, a mechanical method involved attaching a small cap to a 'cocainized eye' [1]; today techniques such as electro-oculography, scleral search coil, dual-Purkinje trackers and video-based methods provide ways to serve researchers' needs in contemporary studies. All of these techniques have inherent merits and flaws. They are filled with tradeoffs in comfort, accuracy, noise, cost, ease of calibration, suitability to a large population, and so forth. None of them completely satisfies the diverse necessities of researchers. Because of its minimal obtrusiveness to observers, relatively easy set-up and reliance on rapidly developing optical and electronic imaging devices, video-based eye tracking has become one of the most popular eye-tracking techniques.

* Corresponding author. Email: pelz@cis.rit.edu

Video-based eye tracking systems use a video camera to image the eye. Based on how this 'eye camera' is positioned, video-based eye tracking systems can be divided into two categories: head-mounted and remote. Head-mounted eye trackers typically include an additional camera to image the scene in which the subject is looking while remote trackers commonly operate in accordance with a computer monitor on which the subject is performing a task. Head-mounted video-based eye trackers have an optical module set on a headgear worn by the user. They are, to some extent, more intrusive than remote trackers but provide the observer with more freedom of motion. The recent rapid improvements in compact electrical and optical components have greatly reduced the size of head-mounted modules (e.g. [2, 3]). On the other hand, remote video-based eye trackers have the eye camera mounted remotely on another base, which can be completely unobtrusive at the sacrifice of overall flexibility. For further reading about eye tracking techniques, earlier reviews [5, 6] and more recent critical surveys [7-10] provide valuable information.

Video-based eye tracking techniques have become increasingly attractive in many research fields, such as visual perception, ocular diagnosis and human-computer interface design. One of the dramatic impacts from the success of video-based eye trackers – especially those using head-mounted optics – is that they provide the opportunity to extend eye movement studies from controlled laboratories to more natural environments. These studies can be accomplished by allowing relatively unrestrained eye, head and body movements. For example, Michael F. Land and his colleague [11] worked on finding the viewing strategies when a driver steers, using a head-mounted video system to simultaneously record both the road and the driver's eye. They found that drivers pay attention to the 'tangent point' on the inside of curves; drivers search for this point 1-2 seconds before each bend and return to the point throughout the bend. Other studies for understanding how humans perform everyday extended tasks include making tea [12], hitting the ball in cricket [13] and hand-washing [14]. For a survey of using eye tracking in studying natural behaviours, see [15]. Applications of eye tracking techniques in a broad range of fields have been recently reviewed in [8].

With the increased flexibility of head-mounted eye trackers come artefacts in output eye-in-head orientation as the subject is freed to move through the environment. These artefacts arise as a result of translational movements of the eye tracking camera with respect to the subject's eye, which produce displacements of the pupil and CR in the eye images that are mistakenly attributed to eye-in-head rotational movements. If the headgear were perfectly stable and moved exactly with the subject's head, and the eye camera and scene camera were securely mounted onto the headgear, the cameras would not move with respect to the subject's eye and any displacement of the pupil or CR within the eye images would be due solely to rotational eye movements. Unfortunately, this idealistic scenario does not exist. The headgear may move a small amount – e.g. bob up and down as the subject walks or simply when the subject makes a facial expression – and small movements of the headgear have a large affect on the output eye-in-head orientation. A 0.1 mm movement of the eye camera with respect to the eye will introduce an artefact of about 1° in the output eye orientation ([6], pp. 415- 416). Additionally, video-based eye trackers suffer from inaccuracies in CR detection due to the CR rolling off the cornea (onto the sclera) during large rotational eye movements, or spurious reflections being mistaken for the desired CR (reflection of the eye tracker's illumination source). We present two applications for solving these problems; the foundation of these applications is comprised of two values which we term the rotational and translational gains.

The rotational gain refers to how much the CR is displaced in an eye image for a unit displacement of the pupil during a rotation of the eye in the head. It is these eye-in-head rotations that we wish to extract from the eye tracking data to determine how a subject is moving his eyes. The rotational gain provides the ability to predict where the desired CR will be located in an eye image based on its previous location and the amount the pupil has moved between the last and current image (see Section 6.2). Prediction of CR position allows for distinguishing the desired CR – the actual reflection of the eye tracker's illumination source – from

spurious reflections that may result in artefacts in the final eye-in-head output (when a spurious reflection is mistaken for the desired CR).

The translational gain, on the other hand, refers to the amount the CR is displaced in an eye image when the pupil is displaced one unit due to a translation of the eye. With head-mounted eye trackers, these translational eye movements are the result of the eye tracking headgear moving with respect to the subject's eye. It is these translational movements that we wish to remove from the eye-in-head results. Separation of rotational movements from translational movements allows for a less noisy output eye-in-head angular orientation than if these translational movements were not compensated (see Section 6.1).

With portable eye trackers, we are concerned with how the eye is moving within the head and using this data to determine where, within a series of scene images, the subject is looking. Since the headgear moves with the subject's head and the scene camera is attached to the headgear, we do not need to determine how the head itself is moving. It is the relative motion between the headgear (specifically, the eye tracking camera) and the subject's eye that we are concerned with. This motion is constrained to small movements (when the headgear is strapped to the head, as in the cases of [2, 3]) that can be approximately modelled as translational movements with respect to the eye. These movements, in fact, doubly affect the gaze position marked in the scene image as they also describe how the scene camera is moved; in this paper, our focus is on improving determination of the rotational eye movement within the head and not the gaze position in the scene images. In other words, we aim at improving the determination of the eye-in-head angular orientation before it gets mapped to the observer's point-of-regard in the scene images. Estimation of translational camera movement may also be applied after this mapping to improve output point-of-regard but that is beyond the scope of this paper.

This paper first provides an overview of basic techniques in video-based eye tracking. The physiological optics used for calculating the reflection of an illumination source (corneal reflection) and the image of the pupil centre (apparent pupil centre) are introduced in Section 3 as necessary background towards understanding our derivations of the rotational and translational gains. These gain values are then derived in Section 4 for two illumination conditions: collimated and near-source illumination. An empirical validation of these gain values – important given the approximations and simplifications used in Section 4 – is provided in Section 5. Section 6 includes our two applications of using these gain values in video-based eye tracking: (1) removal of artefacts in eye-in-head orientation due to translational movements, and (2) prediction of CR position to eliminate artefacts due to spurious reflections. Our second application also includes a description of a new apparatus that produces multiple intentional CRs (from illumination sources on the eye tracking headgear) permitting the tracking of a larger range of eye movements. We conclude this paper in Section 7.

2. Video-based eye tracking

Typical video-based eye tracking systems simultaneously record an image of the pupil and the *corneal reflection of an illumination source* (CR). Although the pupil and CR as seen in an eye image are both sensitive to translational eye movements with respect to the eye camera (caused by headgear slippages, sensor movements, muscular tremors, etc.), their *positional difference vector* (P-CR) provides a signal that changes primarily with rotational eye movements in the head [16] (figure 1). As such, this video-based technique is moderately tolerant of translational movements of the eye with respect to the eye camera, which may be serious problems in some other reflected-light-based techniques (e.g. limbus eye trackers). For brevity, from this point on, we will refer to the two movements often 'seen' by the eye tracker as *rotational movements* and *translational movements*, respectively, where rotational movements refer to rotational eye movements in the

head and translational movements refer to translational eye movements with respect to the eye camera (see figure 1). With our RIT Lightweight Eye Tracker [2] (figure 2) – and others like it [3, 4], whose eye camera is mounted on eyeglass frames – translational movements are especially severe to the output eye-in-head position due to the close proximity of the camera and illumination source to the eye (as compared with other trackers whose illumination sources are further away or collimated by additional optics). This lightweight tracker constrains camera movements largely to horizontal and vertical translational motions as the eyeglass frames are firmly situated on the subject's nose and ears via a strap that goes around the head (strap not shown in figure 2) and the cameras are securely mounted to prohibit rotational movements about their axes. Note, as mentioned previously, that we are not concerned with head movements as we are interested in the eye-in-head angular orientation. Accordingly, the optical derivations provided in Section 4 are most applicable to lightweight eye trackers with cameras mounted on eyeglass frames.

[Insert figure 1 about here]

Near infrared (IR) illumination is commonly used in video-based eye tracking. IR provides the benefit of being invisible to humans so it does not disturb or distract the observer. Additionally, the iris reflects strongly in the near IR, irrespective of iris colour. The strong IR reflectance yields high contrast images which are particularly beneficial to pupil detection. Collimated and near-source illuminations are two conventional approaches for illuminating the eye. In the former approach, parallel rays are either emitted from a distant illumination source, which is approximately the situation for a remote eye tracker, or collimated by optical components, which is the case in some head-mounted eye trackers. In other illumination schemes, such as with the RIT Eye Tracker (figure 2) the illumination source is mounted at a finite distance (typically 50mm or less) from the eye and there is no optical component between the source and the eye to collimate the rays. Thus rays illuminating the eye are not parallel; we use the term *near-source illumination* to refer to this condition.

[Insert figure 2 about here]

3. Physiological optics

3.1 Simplified schematic eye

The Gullstrand Number 2 Simplified Eye [17] was used to derive all optical relationships in this paper. This simplified model consists of three refracting surfaces: a single spherical surface with a radius of 7.8mm representing the whole cornea, and the anterior and posterior surfaces of the lens. All refracting surfaces are assumed to be coaxial, with the optical axis of the eye passing through the centre of curvature of each element. The pupil is centred at the anterior surface of the lens 3.6mm away from the corneal vertex. The refractive index of the aqueous humour is equal to 1.333. This eye model does not include the eye's rotational centre; its distance from the corneal vertex is given in Cornsweet and Crane's paper [18] describing a dual-Purkinje eye tracker (a high sampling rate, high accuracy eye tracker that utilizes the 1st and 4th Purkinje images to map the line of sight). Also, the rotational centre of the eye is assumed to be on the optical axis of the eye. The parameters of the eye model and their symbols used in this paper are summarized in table 1. Other symbols used in this paper are listed in table 2.

[Insert table 1 about here]

[Insert table 2 about here]

3.2 Image of an illumination source – corneal reflection

A CR – also known as the first Purkinje image – is a virtual, erect image of an illumination source formed by the cornea. Because the radius of the cornea (r = 7.8mm) is much less than that of the eye (R = 13.5mm), the CR will move in the same direction as the eye rotates. As shown in figure 3, the cornea serves as a spherical, convex surface in the image formation process.

[Insert figure 3 about here]

The CR position can be calculated by using the thin lens equation for paraxial rays [19]:

$$\frac{1}{s}+\frac{1}{s'}=\frac{1}{f}=\frac{1}{r/2} \tag{1}$$

where $f = r/2$ is the focal length of the corneal surface when seen as a reflector. Note, if the illumination source is moved out to infinity ($s=\infty$) – a condition for which rays are collimated – its image will lie in the focal plane of the cornea; the CR is located at $s'=r/2$ from the corneal vertex. Additionally, the CR will be in line with the ray that goes through the corneal centre of curvature.

3.3 Apparent pupil centre

The apparent pupil (entrance pupil) is the image of the actual pupil formed by rays refracted by the cornea, which acts as a concave surface diverging the rays (figure 4).

[Insert figure 4 about here]

Based on the refraction equation of spherical surfaces for paraxial rays [19], the location of the centre of the apparent pupil can be obtained by the following calculation:

$$\frac{n'}{p}+\frac{n}{a}=\frac{n-n'}{r}\Rightarrow a=3.05\text{mm} \tag{2}$$

where p = -3.6mm according to the sign convention in [19].

Note that the apparent pupil centre always falls on the optical axis of the eye, no matter whether the eye translates or rotates, because the actual pupil centre and rotational centre of the eye are assumed to be on the optical axis of the eye. In the following sections, for brevity, we will use the term *pupil centre* with the understanding that we are referring to the apparent pupil centre.

4. Optical relationships between pupil and CR offsets

Considerable variations exist between individuals in terms of surface curvatures, component separations and axial length (~10%) [20]. However, the following optical derivations based on the simplified eye model were experimentally validated for five observers using the RIT Eye Tracker in Section 5 and two applications that benefit from these derived values are provided in Section 6.

Since video-based techniques track the pupil and CR to determine eye orientation, it is beneficial to understand the relationship between these two features during different types of eye movements; these relationships will be manifested in two values that we term the translational and rotational gains. The utilization and benefits of these values will be made clear in Section 6. In the remainder of this section we derive these two gain values. The translational gain refers to the amount the CR moves when the pupil centre

moves one unit due to a relative translational movement between the eye and the eye camera. The rotational gain refers to the amount the CR moves when the pupil moves one unit due to a rotational eye-in-head movement. We start with deriving these gain values for the case of collimated illumination. Following this derivation, we present a more general derivation for near-source illumination which can be extended for an illumination source at any distance from the eye.

4.1 Collimated illumination

4.1.1 Translational gain. Without losing generality, the original eye position is assumed to be centred so that the CR is situated at the focal point of the cornea. As seen in figure 5, for collimated illumination, the CR remains on the focal point of the cornea when the eye is translated from A to A′ (equivalent to a translational camera movement, with respect to the eye, in the opposite direction). The pupil centre also has a translational displacement that is equal to the eye translational displacement. Therefore, when the eye translates with respect to the camera, the pupil centre and CR move the same amount. In other words, the translational gain, g_{trans}, is unity as described in the following equation:

$$g_{trans} = \frac{\Delta c}{\Delta p} = \frac{x}{x} = 1.0 \tag{3}$$

where x, Δc and Δp are the eye translational displacement, the offset of the CR and the offset of the pupil centre, respectively. Based on this result, video-based eye tracking techniques utilize the P-CR vector so that, in the case of collimated illumination, translational eye movements do not contaminate the measure of eye angular orientation.

[Insert figure 5 about here]

4.1.2 Rotational gain. When the eye rotates to a new position A′, the CR is situated at the intersection point of the focal plane of the cornea and the ray, in the direction of the illumination, going through the corneal centre of curvature (see section 3.2) as shown in figure 6.

[Insert figure 6 about here]

The offset of the pupil centre and that of the CR are represented in the following equations:

$$\begin{aligned} \Delta p &= (R-a)\sin\theta \\ \Delta c &= (R-r)\sin\theta \end{aligned} \tag{4}$$

where θ is the rotational angle of the eye.

The rotational gain, g_{rot}, is the ratio of these two offsets which is computed (using values in table 1) as:

$$g_{rot} = \frac{\Delta c}{\Delta p} = \frac{(R-r)\sin\theta}{(R-a)\sin\theta} = \frac{(R-r)}{(R-a)} \approx 0.55 \tag{5}$$

Based on this value, the CR moves about half the distance as does the pupil centre during an eye rotational movement because the pupil centre is located at approximately twice the distance of the corneal centre of curvature from the eye rotational centre.

4.2 Near-source illumination

In the near-source illumination condition, the translational and rotational gain values derived in the previous section are no longer valid. In order to derive new values for near-source illumination, we make two assumptions:

(1) The CR is located in the focal plane of the cornea;

(2) The illumination source is a point source.

The first assumption is only true for a distant illumination source (see Section 3.2). However, for the typical usage with near-source illumination (i.e. source mounted about 30-40mm away from the eye) in the RIT Eye Tracker and given the fact that there are considerable variations between individuals' eyes (~10% [20]), this approximation is reasonable as we will see in Section 5. Without losing generality, the axis of the illuminator is assumed to be positioned directly in line with the optical axis of the initial eye position in our derivations.

4.2.1 Translational gain. In a near-source illumination design, after a translational movement, the CR will not lie at the focal point of the cornea except when the line of sight goes through the illuminator (original eye position in figure 7).

[Insert figure 7 about here]

As before, the position of the CR after an eye translation is estimated as the intersection point of the ray passing through the corneal centre of curvature with the focal plane of the cornea. Because the triangles STT′ and SCC′ are similar, as shown in figure 7, the translational gain for any position of an illuminator is calculated as:

$$g_{trans} = \frac{\Delta c}{\Delta p} = \frac{r/2 + s}{r + s} = \frac{3.9\text{mm} + s}{7.8\text{mm} + s} \tag{6}$$

For s equal to 30mm and 40mm (approximate limit values in implementations of the RIT Eye Tracker), g_{trans} is equal to 0.90 and 0.92, respectively. These two values are significantly lower than unity, the translational gain in the case of collimated illumination.

Figure 8 shows the translational gain plotted as a function of the position of the illumination source using equation (6). This plot indicates that using the P-CR vector cannot fully eliminate the contamination of translational eye movements unless the illumination source is far away from the eye (or the rays are collimated by additional optics). As the source is moved further from the eye, the translational gain approaches unity, which is the value under the condition of collimated illumination. Therefore, the translational gain in Section 4.1.1 can be considered as a special case of that derived in this section (equation (6)). This equation can be used to determine how far away a remote tracker must be in order to use the P-CR method based on the accuracy desired.

[Insert figure 8 about here]

4.2.2 Rotational gain. As in the previous section, the CR position after the eye moves is estimated as the intersection point (T′ in figure 9) between the focal plane of the cornea and the ray passing through the corneal centre of curvature.

[Insert figure 9 about here]

Because the pupil centre is still located on the optical axis of the eye in the new eye position (see Section 3.3), the pupil offset when the eye rotates can be described by the same equation as equation (4):

$$\Delta p = (R - a)\sin\theta \tag{7}$$

In the new eye position, the illumination source becomes an off-axis object, and its object distance is

$$s' = (s + R)\cos\theta - R \tag{8}$$

Note in figure 9, that S′ is the projection of the illumination source on the optical axis of the eye after the eye rotates, and the vector $\overline{SS'} = d$ is computed by using the trigonometric relationship in the right-angled triangle SES′:

$$d = (s + R)\sin\theta \tag{9}$$

Similarly, the projection of the CR on the optical axis of the eye lies on the focal point (F′) of the cornea. The right-angled triangles T′C′F′ and S C′S′ are similar, so we get:

$$\frac{t}{d} = \frac{C'F'}{C'S'} = \frac{r/2}{r+s'} \Rightarrow t = \frac{rd}{2(r+s')} \tag{10}$$

Based on the triangle T′W′F′, we get:

$$y = \overline{W'F'} = \frac{t}{\tan\theta} = \frac{rd}{2(r+s')\tan\theta} \tag{11}$$

The vector $\overline{EW'} = \overline{EF'} - \overline{W'F'}$, so:

$$x = \overline{EW'} = \overline{EF'} - y = (R - r/2) - y = (R - r/2) - \frac{rd}{2(r+s')\tan\theta} \tag{12}$$

The displacement of the CR in an eye image is equal to:

$$\Delta c = x\sin\theta = \left[(R - r/2) - \frac{rd}{2(r+s')\tan\theta}\right]\sin\theta \tag{13}$$

Inputting equations (8) and (9) into equation (13), we get:

$$\Delta c = \left[(R - r/2) - \frac{r(s+R)\sin\theta}{2[r + (s+R)\cos\theta - R]\tan\theta}\right]\sin\theta \tag{14}$$

For simplification, we assume small rotational eye movements for which θ is considered as within ±10˚. Thus, we have the following approximations (error introduced is 1% or less if θ is 10˚ or less):

$$\begin{aligned} \sin\theta &\approx \theta \\ \tan\theta &\approx \theta \\ \cos\theta &\approx 1 \end{aligned} \tag{15}$$

Inputting these equations into equation (14), we get:

$$\Delta c = \left[(R - r/2) - \frac{r(s+R)\theta}{2[r + (s+R) - R]\theta}\right]\theta \tag{16}$$

Finally, the rotational gain for any position of an illuminator is equal to:

$$g_{rot} = \frac{\Delta c}{\Delta p} = \frac{\left[(R - r/2) - \frac{r(s+R)}{2(s+r)}\right]\theta}{(R-a)\theta} = \frac{R - r/2}{R-a} - \frac{r(s+R)}{2(R-a)(s+r)} \tag{17}$$

Inputting values from table 1 into equation (17), the functional relationship between the rotational gain and the position of the illumination source is represented as (where input values are in millimetres):

$$g_{rot} = 0.92 - \frac{0.37(s+13.5)}{s+7.8} \tag{18}$$

When s is equal to 30mm and 40mm (approximate limits of s for the RIT Eye Tracker), g_{rot} is equal to 0.49 and 0.51, respectively. The plot in figure 10 graphically shows the functional relationship between the rotational gain and illumination source position described in equation (18). As we can see, as the illumination source is moved further away from the eye, the rotational gain approaches 0.55, which is the value we get for collimated illumination. Therefore, as with the translational gain, the rotational gain in the collimated illumination condition is a special case of that in the near-source condition.

[Insert figure 10 about here]

5. Experimental validation*

An experiment was conducted to measure the rotational and translational gains of five observers for the RIT Eye Tracker utilizing near-source illumination.

5.1 Method

The observers were three males and two females ranging in age from 19 to 49 (average 23.6); all had normal or corrected-to-normal vision. The experiment consisted of two tasks: (1) looking sequentially through a 3×3 grid of fixation points; (2) fixating on the centre fixation point while moving the eye tracker's headgear. Data from the first task were analysed to determine each observer's rotational gain while data from the second task were analysed to obtain each observer's translational gain. A third task was conducted for validation of a camera movement extraction algorithm and will be discussed in Section 6.1. Each observer sat 3m away from a screen on which the fixation points were projected. Each fixation point was the letter 'X' subtending a viewing angle of approximately 0.5 degrees and separated to elicit rotational eye movements of 10 degrees in the horizontal direction and 8 degrees in the vertical direction.

During the experiment, each observer wore the RIT Lightweight Eye Tracker (see figure 2); this eye tracker uses an infrared emitting diode (IRED) that is mounted close to the eye camera and illuminates the eye from a distance of about 30-40mm (depending on the individual's face). Video streams from the eye tracker's two cameras (eye and scene cameras) were sent through a multiplexer in a backpack and recorded by a camcorder. Following the data collection, the recorded videos were demultiplexed and run through an ISCAN 726/426 Pupil/Corneal Reflection Analysis System [22]. Horizontal pupil and CR data output by the system were used to determine the rotational and translational gains. Vertical data analysis is similar and will not be discussed in the following sections.

5.2 Rotational gain measurement

Observers were asked to keep their heads and the eye tracking headgear stationary while they looked through the nine calibration points, one at a time, making horizontal eye movements between the points in each row and vertical movements between the three rows of points. Data from one observer for this trial are shown in figure 11. A linear regression was performed on the pupil and CR horizontal data collected during this task to determine the rotational gain value. See figure 12 for an example regression performed on one observer's data. The slope of the best-fit line is taken as the observer's rotational gain. Results for all observers are shown in table 3 along with the R^2 value for each regression. These R^2 values are presented to demonstrate

* The material in Sections 5 and 6.1 was presented in [21]. In [21], the rotational and translational gains are referred to as eye and camera gains, respectively.

the validity of performing a linear regression as well as the constancy of the gain values throughout the duration of the eye movements.

[Insert figure 11 about here]

[Insert figure 12 about here]

The rotational gains calculated in Section 4.2.2 ranged from 0.49 with the IRED 30mm away to 0.51 with the IRED 40mm away from an eye with a corneal radius of 7.8mm. As shown in table 3, the rotational gain values calculated from the five observers ranged from 0.48 to 0.55 with a mean of 0.51 and standard error of 0.01; this mean value matches that derived in Section 4.2.2. The variations are most likely due to variations in the radii of observers' corneas [20] as well as the distance of the IRED to each observer's eye. Therefore, despite the assumptions and simplifications made in deriving these values in Section 4.2.2, the derived values do closely approximate those determined experimentally.

[Insert table 3 about here]

5.3 Translational gain measurement

Observers were asked to fixate on the centre fixation point and, while keeping their eyes and heads still, move the eye tracker's headgear. The headgear (along with its attached cameras) was shifted horizontally and vertically over a range of approximately 18 millimetres. A 25-second segment of data from one observer for this trial is shown in figure 13. As with the rotational gain, the translational gain was measured by performing a linear regression on the pupil and CR data from this trial. The data from figure 13 is shown in figure 14 with the best-fit line. The slope of this line is equal to the translational gain for this observer. The translational gains determined for all observers, including the R^2 of the regressions, are shown in table 3.

[Insert figure 13 about here]

[Insert figure 14 about here]

The translational gain values derived in Section 4.2.1 ranged from 0.90 with the IRED 30mm away to 0.92 with the IRED 40mm away from the observer's eye. The values calculated for our five observers ranged from 0.82 to 0.89 with a mean of 0.86 and standard error of 0.01. This mean value is less than the translational gain values derived theoretically. One reason for the lower gain value may be the intrusion of small rotational eye movements during the task. Even when observers attempt to hold the eye as still as possible, there are microsaccades, tremor and drift [6] that will reduce the overall gain. Observers may have also made some rotational eye movements within the fixation point (the letter 'X'). Because rotational eye movements produce a significantly smaller gain value (about 0.51 for these five observers), this likely accounts for the lower observed translational gain values. The effect was particularly noticeable in data from observer 1 (figure 15). A combination of rotational and translational movements will result in an overall gain value (ratio of CR offset to pupil offset) between the rotational and translational gain values derived.

[Insert figure 15 about here]

6. Applications

In this section, we present two applications of the gain values derived in Section 4 and validated in Section 5. Both applications apply to video-based eye trackers; the first describes a method for separating translational camera movements (with respect to the eye) from rotational eye movements (within the head), and the second uses a CR prediction technique to increase the robustness of our new eye tracking system prototype.

6.1 Compensating for translational movement and noise reduction

With the important advantage of portability obtained in head-mounted eye trackers comes the disadvantage of potentially less accurate data due to uncompensated movements of the eye tracking headgear. As the eye camera translates with respect to the eye, the pupil and CR are displaced in the eye image; if this kind of translational movement between the camera and eye is not discerned and compensated, it will result in an apparent rotational eye movement and, consequently, adversely affect the final eye-in-head output. For this reason, it is very important that translational movements be distinguished from rotational movements using the available pupil and CR data.

Currently, most eye tracking systems compensate for translational movements by using the P-CR technique (see Section 2), which uses the simplifying assumption that the pupil and CR move the same amount when the camera translates with respect to the eye. In other words, the P-CR technique assumes a translational gain of unity. However, as was shown in Section 4.2.1, this is only correct in the case of collimated illumination. Other methods to compensate for translational movements have been proposed in the literature [23, 24]. Unfortunately, these techniques require additional image processing, do not fully compensate for translational movements (camera movements with respect to the eye), and suffer from additional artefacts due to any errors and/or noise in localizing the additional landmarks used to compensate for these movements. In these methods, the pupil and CR are used to determine eye orientation while additional features are tracked to determine translational movements introducing more potential for error and/or noise. A method that does not require any additional processing, but instead uses the gain values discussed in Section 4 along with the tracked pupil and CR positions, is presented here.

An additional advantage of this eye tracking method is noise reduction. The CR position array is typically much noisier than the pupil position array due in part to the much smaller size of the CR (see figure 1). Therefore results using the P-CR technique are noisier than they would be if just the pupil position data could be used, as they are at least as noisy as the CR data. In the present technique, the CR data are only used to determine translational movements. Again, these translational movements of the eye in the eye images are the result of camera motion with respect to the eye. Under the assumption that these translational movements are much slower and less frequent than rotational eye movements, camera movement data (representing these translational movements) can be smoothed and then subtracted from the pupil data. Therefore, final eye-in-head data – equal to the pupil position vector minus the camera position vector – will have a noise level comparable to that in the less-noisy pupil position data. The following section will describe the derivation of a new relationship between pupil and CR position that more effectively compensates for translational camera movement and permits noise reduction without degradation in temporal resolution. Following this section is an empirical validation of this algorithm.

[Insert table 4 about here]

6.1.1 Camera movement extraction. The rotational and translational gains (equations (19) and (20)) are the foundation for this algorithm that separates translational camera movement data from rotational eye movement data. The variables used in this section are described in table 4.

$$g_{rot} = \frac{\Delta CR_{rot}}{\Delta P_{rot}} \approx \frac{CR_{rot}}{P_{rot}} \tag{19}$$

$$g_{trans} = \frac{\Delta CR_{trans}}{\Delta P_{trans}} \approx \frac{CR_{trans}}{P_{trans}} \tag{20}$$

For the approximation in the above equations to hold, the value of the P_{track} and CR_{track} vectors when the observer is looking in the centre of his field-of-view should be subtracted from the entire P_{track} and CR_{track} vectors, respectively. To accomplish this in our implementation, we start recording when an observer is looking at the centre of his field-of-view and subtract the first data value in P_{track} and CR_{track} from each of these vectors.

In any video-based eye tracker, the eye camera will not be held strictly constant with the observer's head. Even with the observer on a dental bite-bar, small movements of the head (with respect to the eye camera) may occur, which results in a combination of translational and rotational eye movements affecting the tracked pupil and CR positions:

$$P_{track} = P_{rot} + P_{trans} \tag{21}$$

$$CR_{track} = CR_{rot} + CR_{trans} \tag{22}$$

Assuming the rotational and translational gains are measured or that averages are used (see Sections 4 and 5), we now have four equations (equations (19)-(22)) and four unknowns: P_{rot}, P_{trans}, CR_{rot}, CR_{trans}. In our implementation, we found that the average gains presented in Section 5 were sufficient to calculate rotational and translational movements for all observers. Our goal is to solve for P_{trans} in terms of the four known variables in order to extract and smooth these translational movements. Therefore we start with a rearrangement of equation (21) in terms of P_{trans} (equation (23)) and multiply both sides by the rotational gain, g_{rot}, to obtain equation (24) (after a substitution using equation (19)).

$$P_{trans} = P_{track} - P_{rot} \tag{23}$$

$$g_{rot} \cdot P_{trans} = g_{rot} \cdot P_{track} - CR_{rot} \tag{24}$$

Subtracting CR_{trans} from both sides and making additional substitutions using equations (20) and (22) results in equation (25), which can be rearranged to solve for P_{trans}, as in equation (26):

$$g_{rot} \cdot P_{trans} - g_{trans} \cdot P_{trans} = g_{rot} \cdot P_{track} - CR_{track} \tag{25}$$

$$P_{trans} = \frac{g_{rot} P_{track} - CR_{track}}{g_{rot} - g_{trans}} \tag{26}$$

As described in table 4, this P_{trans} vector represents the amount that the pupil centre has moved in the eye image due to translational movements of the camera with respect to the eye. Since the camera moves infrequently and relatively slowly, this vector may be smoothed before being extracted from the tracked pupil position, P_{track}, without adverse affect. This allows for reduction of noise due to CR position estimation without loss of information about rotational eye movements because P_{trans} contains no information about rotational eye movements, only translational movements between the eye and the camera. In sum, this technique uses CR position data to correct pupil position data such that the output pupil position data, P_{rot}, represents only rotational eye movements.

6.1.2 Algorithm verification. The camera movement extraction algorithm was tested using the same experimental setup described in Section 5.1. The same five observers looked through the nine fixation points while moving the camera as described in Section 5.3. Pupil and CR data output from the ISCAN analysis system for one observer during this trial are shown in figure 16; these data were then run through this algorithm to separate rotational eye movements from translational eye movements due to camera motion. Average gain values presented in Section 5 were used to calculate P_{trans}; to use this algorithm with a different eye tracker, one could determine the gain values of that eye tracker either through experimentation as described in Section 5.1 or calculation using measured distance between eye and IRED (equations (6) and (18)).

[Insert figure 16 about here]

In this section, *Camera vector* refers to P_{trans} and *Eye vector* refers to P_{rot}. The Camera vector was calculated using equation (26) then smoothed with a median filter of width 7 fields (1 field = 1/60 second) followed by a Gaussian filter with a standard deviation of 4 fields. These smoothed camera data were then subtracted from the raw Pupil data to create an Eye vector describing the amount the pupil moved due to rotational eye movements only. The final Eye and Camera vectors for the data shown in figure 16 are shown in figure 17.

[Insert figure 17 about here]

For comparison, the P-CR vector – used by the ISCAN system to determine eye position – is shown alongside the Eye vector in figure 18. During this segment of data, the observer was instructed to look through three horizontally displaced fixation points. Therefore, a vector describing just the rotational eye movements should appear (when plotted against time) as horizontal lines during fixations on each point with a large slope as the eye saccades between fixations. An affect of the camera movement can be seen in the P-CR vector during the fixations; for instance between two and five seconds in figure 18, the P-CR data fluctuates about zero degrees as the observer is fixating on the centre fixation point while the Eye vector shows the horizontal position remaining relatively constant (i.e. the observer is holding fixation). Therefore smoothing the Camera vector does not have the effect of merely high-pass filtering the Eye vector, as this low frequency affect of camera movement is removed. Additionally, it is important to note that the smoothing of the Camera vector does not result in loss of small rotational eye movement information. In figure 18, between one and two seconds as the observer looks from the first point in the row to the second, he makes a small saccade which can be seen clearly in the Eye vector even though the Camera vector has been smoothed. A zoomed-in view of this section in figure 18 between one and two seconds is shown in figure 19b.

[Insert figure 18 about here]

[Insert figure 19 about here]

Figure 19 also compares the Eye and P-CR vectors to the Pupil and CR vectors. The P-CR vector is calculated directly by subtracting the CR vector from the Pupil vector and therefore contains at least as much noise as is present in the CR vector. The Eye vector, on the other hand, is calculated by subtracting a smoothed Camera vector from the Pupil vector and therefore contains only approximately the same noise level as is present in the Pupil vector. Since the Pupil vector tends to be less noisy than the CR vector, the Eye vector is correspondingly less noisy than the P-CR vector.

6.2 Predicting CR locations and artefact removal

In this section, we use the rotational gain derived in Section 4.2 to differentiate desired CRs (actual reflections of the eye tracker's illumination sources) from spurious reflections (reflections of ambient illumination sources) in eye tracking video frames to improve the robustness of our new eye tracking system prototype. In

the new design, we address two limitations of current video-based eye tracking systems: 1) loss of CR during extreme rotational eye movements, and 2) direct and indirect reflections of sunlight on the cornea being mistaken for the desired CR. Towards solving both of these problems, we use an array of illuminators (3×3 IREDs), which we term 'structured illumination', to illuminate the eye. The IREDs, mounted on a piece of supportive plexiglass in front of the eye, intentionally produce multiple CRs in eye images to ensure that – even with extremely eccentric gazes – we can obtain at least one trackable CR (a CR superimposed on either the pupil or iris). This method avoids track losses caused by a single CR "rolling off" the cornea and onto the irregular sclera due to very large rotational eye movements (as do the leftmost CRs in figure 20b). Thus, the measurement range of the system is improved dramatically.

Two sample eye images generated by the new system are shown in figure 20. Note that some CRs are visible even during an extreme rotational eye movement. However, many artefacts are observed in the images and more artefacts may be seen under daylight. These artefacts may be due to reflections of multiple illuminators, extraneous ambient illumination and the aspherical curvature at the edges of the cornea. The challenge of removing these artefacts is solved by a two-stage processing approach. First, global and local statistical information of an eye image are utilized to isolate and determine the pupil centre and potential CRs. Second, desired CRs are distinguished from potential CRs by a CR prediction technique using the rotational gain derived in Section 4.2.2. We define the *desired CRs* as the reflections of the 9 IREDs on the eye tracker's headgear and *potential CRs* as features in the eye images resembling desired CRs (either due to spurious reflections or image artefacts).

[Insert figure 20 about here]

6.2.1 Detection of potential CRs and the pupil. An eye image is first smoothed by a Gaussian filter followed by selection of the brightest pixels in the image (top 1% of pixel values); CR pixels are among these brightest pixels. After a region labeling operation, connected components larger than 0.15% of the image size of the eye image are eliminated. Additional spurious specular reflections are removed by a local contrast technique, which only accepts potential CRs that have a high contrast with a small set of their neighboring pixels (figure 21a, b). Before detecting the pupil, these potential CRs are removed from the eye image and the remaining holes are padded with the mean gray values of their surrounding areas. A threshold operation is then applied that selects pupil pixels as those whose values fall below the gray value of the first valley in the image histogram. Afterwards, morphological closing and filling operations are employed to join boundaries and remove holes in all connected components. The pupil region is chosen as the largest connected component in the binary image, excluding the background (figure 21c, d).

[Insert figure 21 about here]

6.2.2 Desired CR discrimination using the rotational gain. As we learned from Sections 4 and 5, the CR moves only about half the distance as does the pupil centre when the eye rotates for collimated or near-source illumination conditions. After rearrangement of equation (19), we obtain:

$$CR_{current} - CR_{previous} = \Delta c = g_{rot}\Delta p \tag{27}$$

$$CR_{current} \approx 0.5\Delta p + CR_{previous} \tag{28}$$

This last equation shows that a displaced CR position can be approximately predicted if the pupil offset between the current and previous frame and the CR position in the previous frame are known.

In our implementation, nine CR positions in the first frame are manually selected. Nine predicted CR locations for each following frame are then calculated based on equation (28). When a potential CR after the first-stage processing falls inside a predefined square (length of side equal to 50 pixels) around a predicted CR

location, it is identified as a desired CR. This square region allows for a small amount of translational eye movement to occur such that the desired CRs will still fit within these regions The region also permits individual variations between eyes when an average rotational gain is used to predict the desired CR positions. If a potential CR does not fall inside this square, it is considered to be an artefact and excluded from the final desired CR list (figure 22). If more than one potential CR satisfies the criterion, other operations may be included, such as averaging the CRs within the predicted region. The circumferences and centres of the pupil and CRs are calculated by a direct least-squares ellipse fitting technique introduced in [25].

[Insert figure 22 about here]

7. Conclusion

Video-based eye tracking is a common technique used to track eye movements. Head-mounted video-based eye trackers allow subjects to perform natural tasks under minimum restraint by the eye tracking apparatus. With the improved flexibility of head-mounted trackers, specifically those mounted on eyeglass frames, comes the possibility of movement of the apparatus that will undesirably affect the tracked eye-in-head (angular orientation) output. This unavoidable effect is the result of tracked eye features – the pupil and CR – being displaced in the eye images due to translational movements of the eye tracking camera with respect to the subject's eye. Therefore, in order to separate these translational movements from rotational eye movements, we have determined the relationships between pupil and CR displacements during these two types of movements. We focus on true rotational eye movements within the head about the eye's rotational centre and translational eye movements due to relative movements between the eye and the eye tracking apparatus. The determined relationships are modelled by two values which we have termed the rotational and translational gains. The knowledge of these values presents the possibility of algorithms to improve video-based eye tracking. We include two such algorithms in this paper.

We first describe the image formation process of the apparent pupil centre and CR. The apparent pupil is the image of the actual pupil as seen by the eye tracking camera through the cornea. The CR is the image of an illumination source formed by the cornea. The distance of the illumination source from the eye plays an important role in the creation of the CR. Hence, the rotational and translational gains are derived for the cases of collimated and near-source illuminations. It was shown that the values derived for collimated illumination satisfy the equation derived for near-source illumination for a source at a great distance. Since the gain values are dependent on the parameters of the eye, they fluctuate with variations in the eyes of individual subjects. Therefore an experiment was conducted to empirically determine the gain values of five individuals.

The rotational and translational gain values are at the heart of our algorithm that separates rotational movements (eye-in-head movements) from translational movements (camera movements with respect to eye) to obtain pupil displacement due only to rotations of the eye within the head. In this algorithm, CR data are used only to determine translational movement in the form of camera position data that can be smoothed under the assumption that the camera moves smoothly and slowly; the smoothed camera position data is then subtracted from the pupil position data. Therefore, the final eye orientation data have approximately the same noise level as the relatively less noisy pupil data. The P-CR technique – a common technique used in video-based eye tracking (see Section 2) – attempts to accomplish this compensation for translational movements under the assumption that the pupil and CR move together during this type of movement (unity translational gain). This assumption was shown to be valid for the case of collimated illumination but not for near-source illumination. Therefore, using the P-CR technique with near-source illuminated eye images results in artefacts in the final eye position data due to translational movements between the eye and eye tracking apparatus. Our algorithm more accurately compensates for translational movements while decreasing the noise in the final eye-in-head rotational data.

The rotational gain value was also used in an algorithm to increase the measurement range and robustness of our new eye tracker prototype. In this algorithm, the rotational gain is used to predict the location of desired CRs. The CR prediction component of this algorithm can be applied to any video-based eye tracking system that tracks the CR. This prediction reduces the threat of spurious reflections being taken as the desired CR, which is a significant problem in video-based eye tracking (especially in daylight).

References

[1] E.B. Delabarre, American Journal of Psychology 9 (1898), pp. 572-574.

[2] J.S. Babcock and J.B. Pelz, paper presented in Proceedings of the 2004 Symposium on Eye Tracking Research & Applications, San Antonio, Texas, USA (2004).

[3] D. Li and D.J. Parkhurst, Journal of Modern Optics. 53 (2006), pp. 1295-1311.

[4] P. Wagner, et al., paper presented in Proceedings of the 2006 Symposium on Eye Tracking Research & Applications, San Diego, California, USA (2006).

[5] L.R. Young and D. Sheena, Behaviour Research Methods & Instrumentation, 7 5 (1975), pp. 397-429.

[6] R.H.S. Carpenter, *Movements of the Eyes*, 2nd edition (Pion Limited, London, 1988).

[7] H. Collewijn, in *Vision Research: A Practical Guide to Laboratory Methods*, edited by R.H.S. Carpenter and J.G. Robson (Oxford University Press, 1999), pp. 245-285.

[8] A.T. Duchowski, *Eye Tracking Methodology: Theory and Practice* (Springer, 2002).

[9] D.C. Richardson and M.J. Spivey, in *Encyclopedia of Biomaterials and Biomedical Engineering*, edited by G. Wnek and G. Bowlin (Marcel Dekker Inc. 2004), pp. 568-572 .

[10] C.H. Morimoto and M.R.M. Mimica, Computer Vision and Image Understanding 98 1 (2005), pp. 4-24.

[11] M.F. Land and D.N. Lee, Nature. 369 6483 (1994), pp. 742-744.

[12] M.F. Land, N. Mennie and J. Rusted, Perception. 28 11 (1999), pp. 1311-1328.

[13] M.F. Land and P. McLeod, Nature Neuroscience. 3 12 (2000), pp. 1340-1345.

[14] J.B. Pelz and R. Canosa, Vision Research. 41 25-26 (2001), pp. 3587-3596.

[15] M.M. Hayhoe and D. H. Ballard, Trends in Cognitive Science. 9 4 (2004).

[16] J. Merchant, R. Morrissette and J.L. Porterfield, IEEE Transaction of Biomedical Engineering, 21 4 (1974), pp. 309-317.

[17] G. Smith and D.A. Atchison, *Eye and Visual Optical Instruments* (Cambridge University Press, 1997), pp 788.

[18] T.N. Cornsweet and H.D. Crane, J Opt Soc Am. 63 8 (1973), pp. 921-928.

[19] E. Hecht, Optics, 3rd edition (Addison Wesley, 1998), pp155-159.

[20] W.N.Charman, in *Handbook of Optics Chapter 24: Optics of the Eye*, second edition (McGraw-Hill Professional, 1994), pp. 24.6

[21] S.M. Kolakowski and J.B. Pelz, paper presented in Proceedings of the 2006 Symposium on Eye Tracking Research & Applications, San Diego, California, USA (2006).

[22] ISCAN, RK-7261PCI Pupil/Corneal Reflection Tracking System, (ISCAN, Inc., 89 Cambridge Street, Burlington, MA 01803, U.S.A., 2001).

[23] F. Karmali and M. Shelhamer, paper presented In Proceedings of the 26th Annual International Conference of the IEEE EMBS, (2004).

[24] X. Xie, R. Sudhakar and H. Zhuang, IEEE Transactions on Systems, Man, and Cybernetics - Part A: Systems and Humans. 28 4 (1998), pp. 487-490.

[25] A. Fitzgibbon, M. Pilu and R.B. Fisher, IEEE Transactions on Pattern Analysis and Machine Intelligence, 21 5 (1999), pp. 476-480.

Table 1: Parameters of the eye model

	Symbol	Value
Refractive index of the air	n	1
Refractive index of the aqueous humour	n'	1.333 (4/3)
Radius of the cornea	r	7.8mm
Focal length of the cornea	f	3.9mm (r/2)
Actual pupil centre from the corneal vertex	p	3.6mm
Apparent pupil centre from the corneal vertex*	a	3.05mm
Rotational centre of the eye from the corneal vertex	R	13.5mm

* The apparent pupil centre is calculated in Section 3.3

Table 2: Some symbols used in this paper

	In Original Eye Position	In New Eye Position
Illumination Source	S	S′
Corneal Vertex	A	A′
CR Position	T	T′
Focal Point of the Cornea	F	F′
Corneal Centre of Curvature	C	C′
Eye Rotational Centre	E	E′

Table 3: Rotational and translational gains with R^2 values (in parenthesis) for each linear regression. SE represents one standard error.

Observer	Rotational gain (R^2)	Translational gain (R^2)
1	0.5161 (0.9990)	0.8178 (0.9786)
2	0.5035 (0.9987)	0.8653 (0.9889)
3	0.5456 (0.9893)	0.8876 (0.9992)
4	0.5120 (0.9992)	0.8760 (0.9960)
5	0.4798 (0.9972)	0.8720 (0.9919)
Mean	0.5114	0.8637
SE	0.0106	0.0120

Table 4: Variables used in camera movement extraction algorithm. All displacements refer to displacements within the eye images. See Section 2 for definitions of rotational and translational movements.

Variable	Data Represented
P_{track}	Raw pupil position data from eye tracker
CR_{track}	Raw CR position data from eye tracker
P_{rot}	Pupil displacement due to rotational movements
CR_{rot}	CR displacement due to rotational movements
P_{trans}	Pupil displacement due to translational movements
CR_{trans}	CR displacement due to translational movements
g_{rot}	Rotational gain
g_{trans}	Translational gain

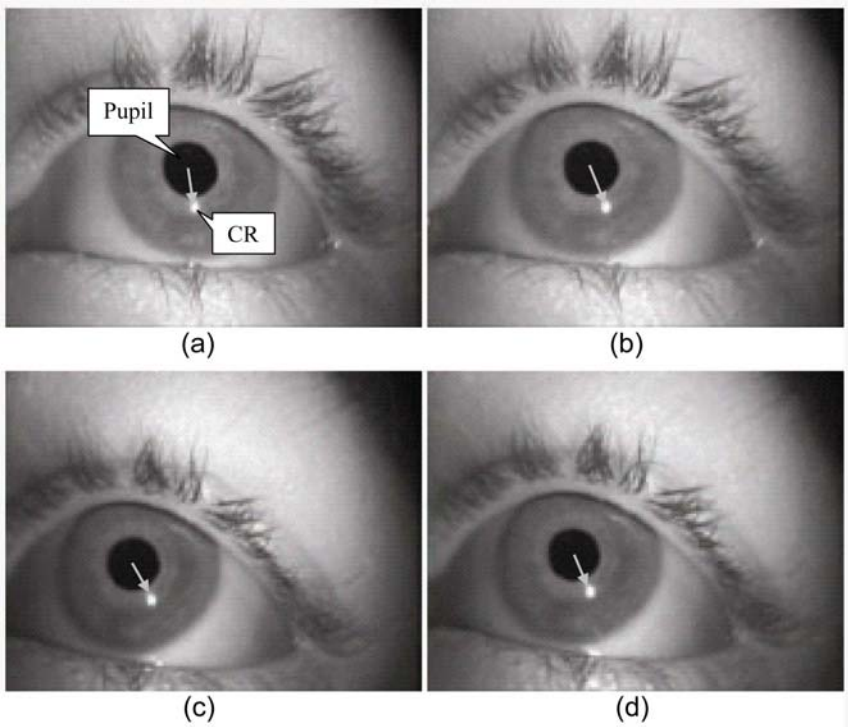

Figure 1: Eye images before (a) and after (b) a rotational eye movement; the P-CR vector has noticeably changed. Eye images before (c) and after (d) a translational eye movement; the P-CR vector has changed only slightly. Images courtesy of [21].

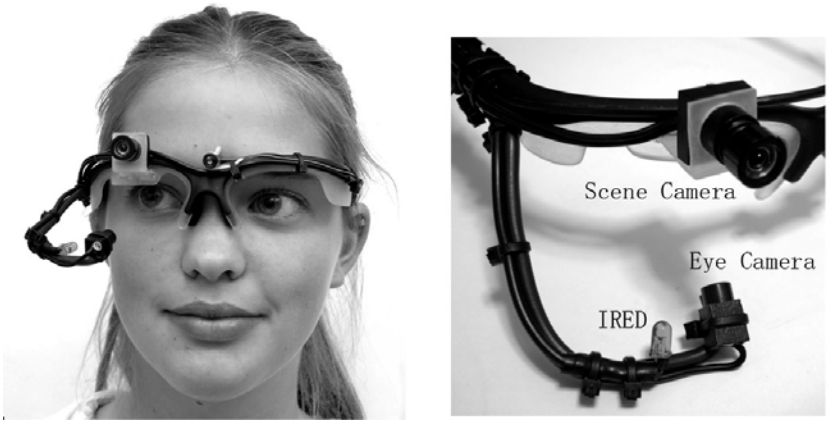

Figure 2: RIT Lightweight Eye Tracking headgear. An infrared emitting diode (IRED) is mounted beside the eye camera about 30-40mm away from the eye. The eye camera captures images of the eye while the scene camera captures what the observer is seeing. Images courtesy of [2].

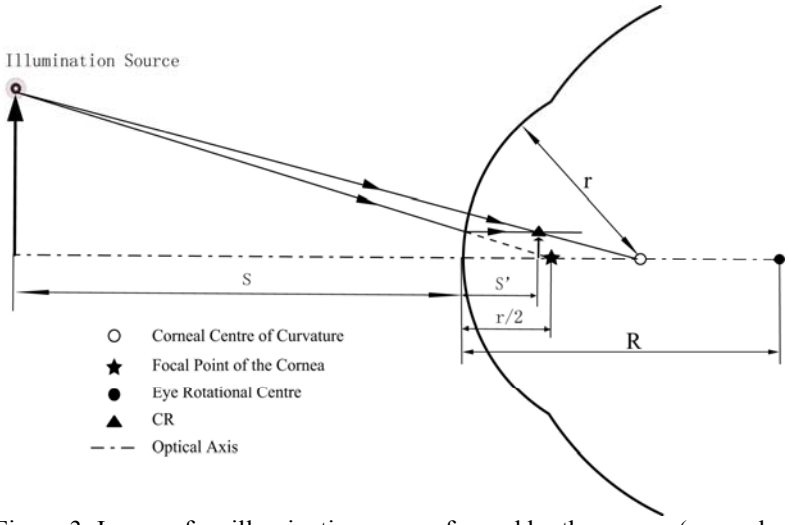

Figure 3: Image of an illumination source formed by the cornea (corneal reflection).

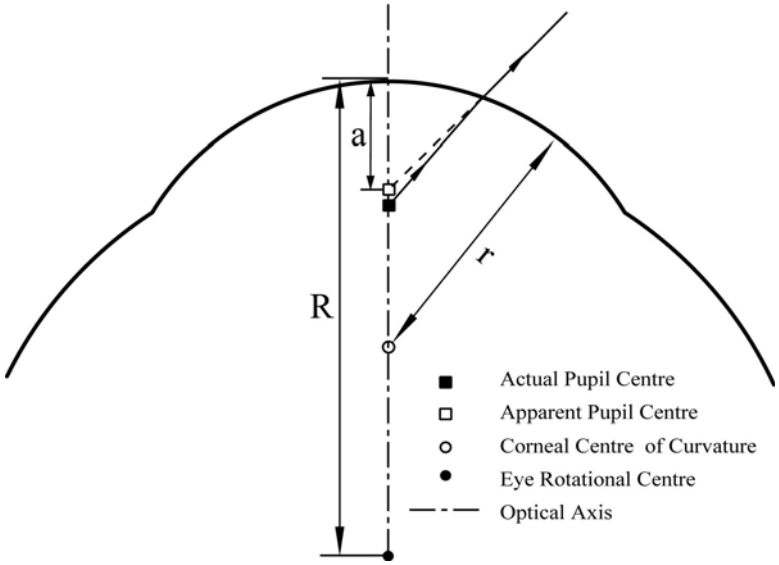

Figure 4: Apparent pupil centre formed by the cornea; it is located at *a*=3.05mm away from the corneal vertex.

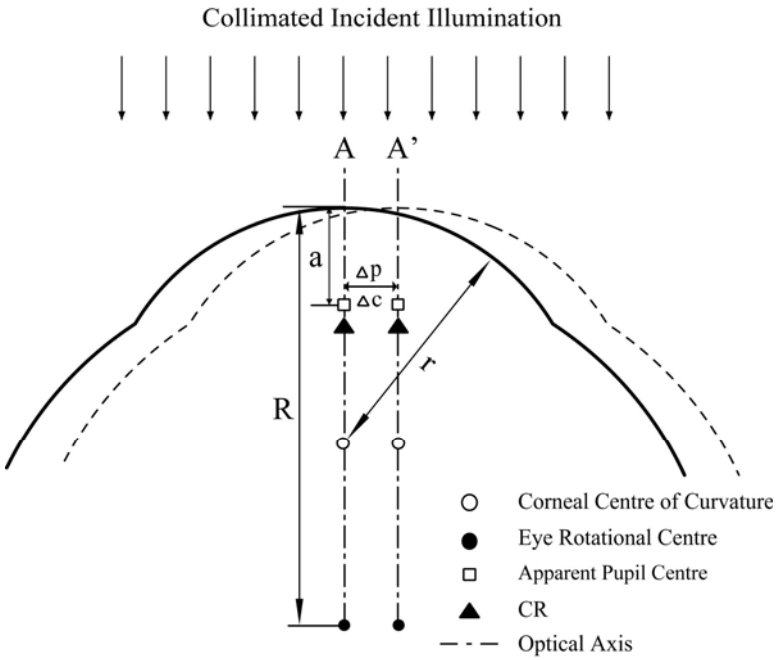

Figure 5: Eye before (solid) and after (dashed) a translational eye movement. The CR and pupil centre move the same amount as the translational eye displacement if the incident rays are collimated; in this case, the translational gain is equal to 1.

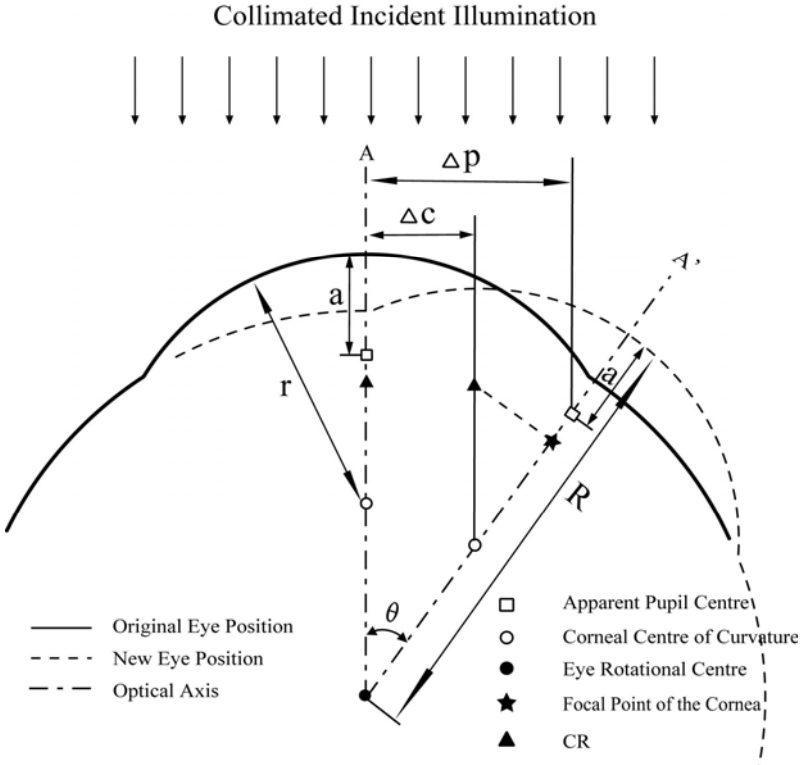

Figure 6: Eye before (solid) and after (dashed) a rotational eye movement. The rotational gain is equal to 0.55 if the incident illumination is collimated. Note that the CR after the eye rotates is located in the focal plane of the cornea in the new position.

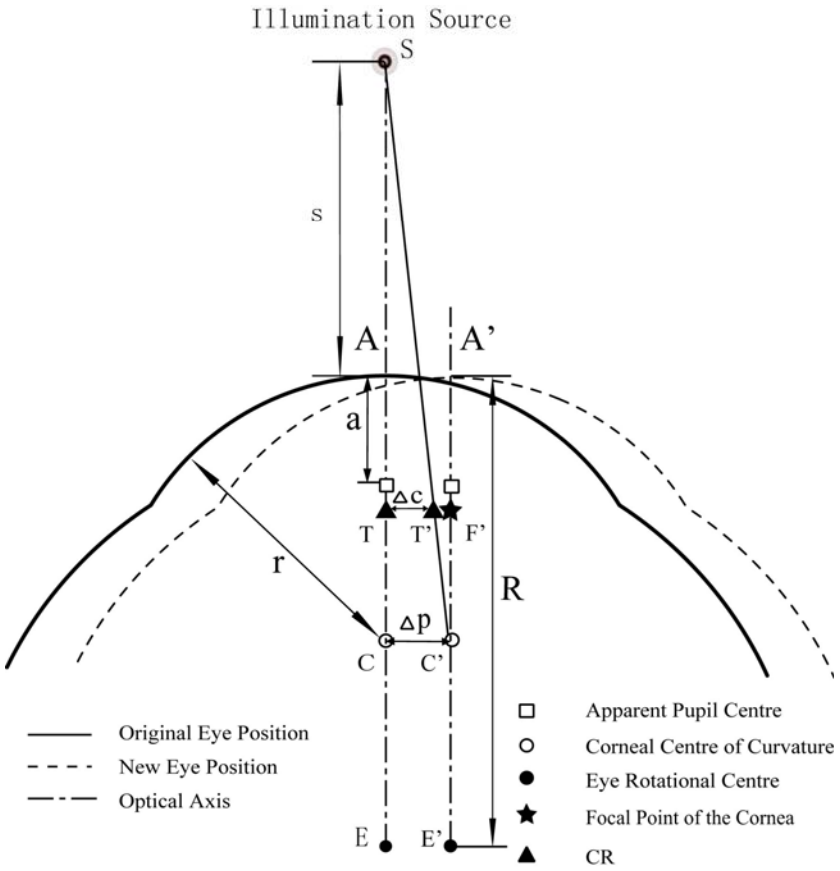

Figure 7: Eye before (solid) and after (dashed) a translational eye movement when the illumination source is close to the eye.

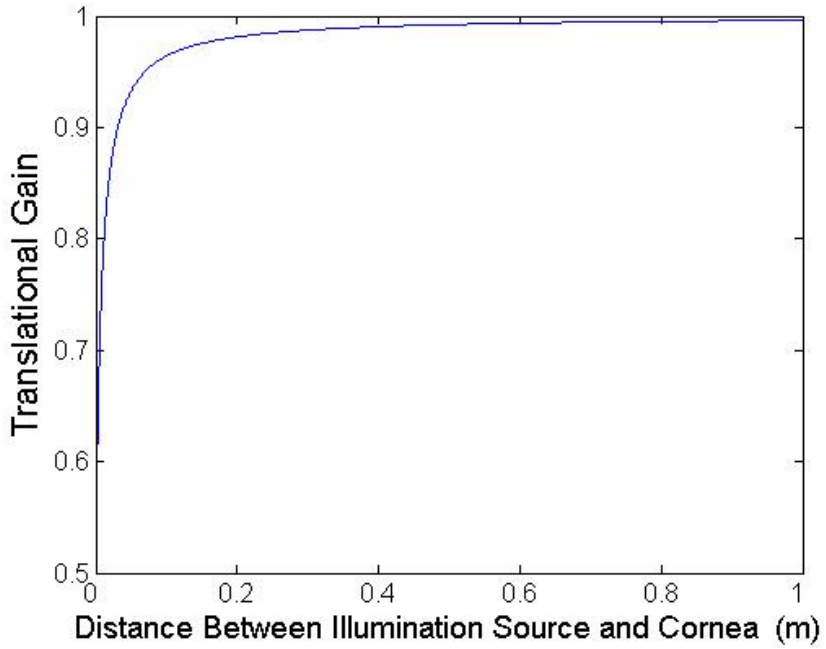

Figure 8: Translational gain versus position of the illumination source (with respect to the eye).

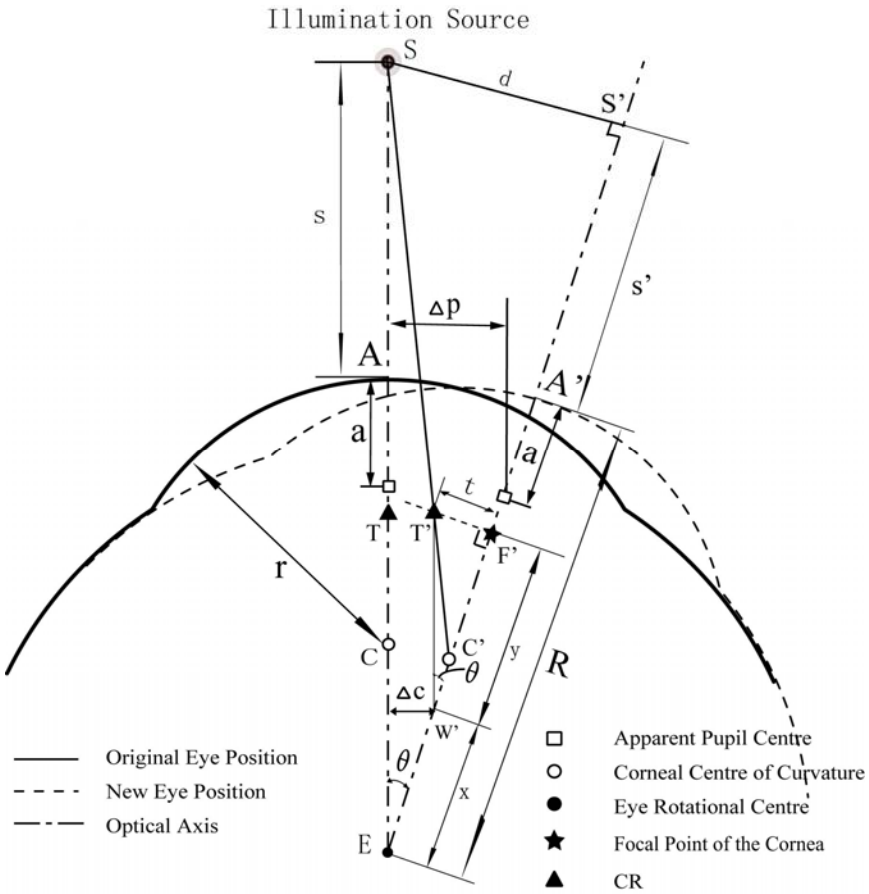

Figure 9: Eye before (solid) and after (dashed) a rotational eye movement when the illumination source is close to the eye.

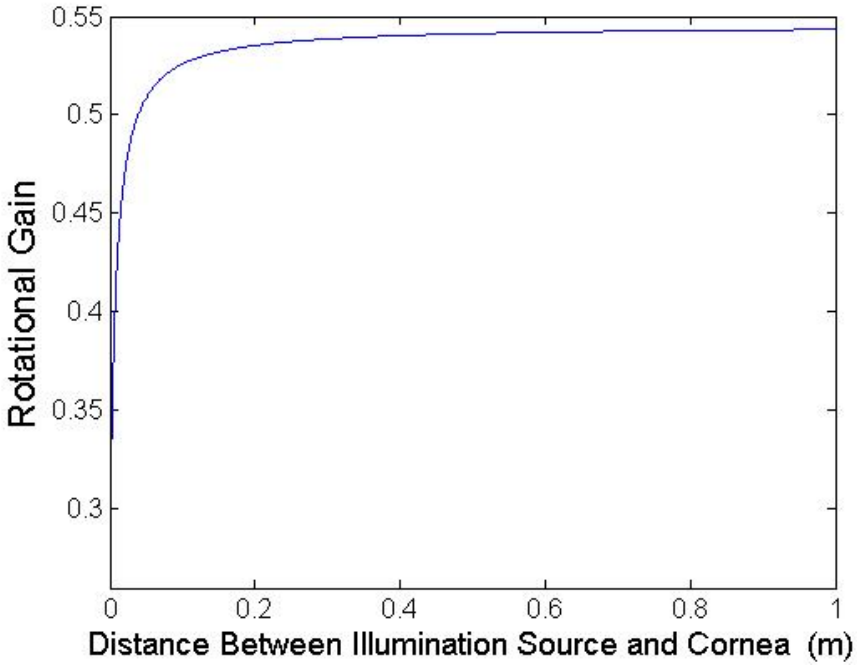

Figure 10: Rotational gain versus position of the illumination source (with respect to the eye).

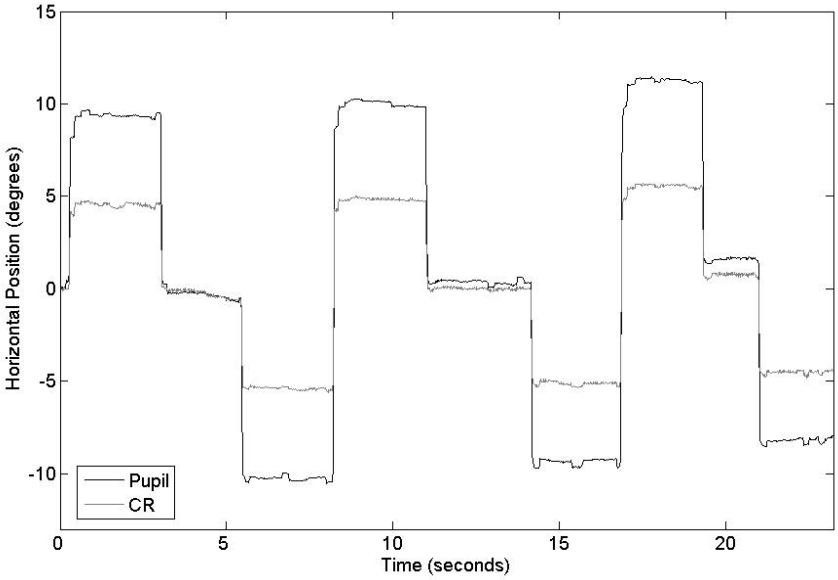

Figure 11: Example data for measuring the rotational gain (observer 4).

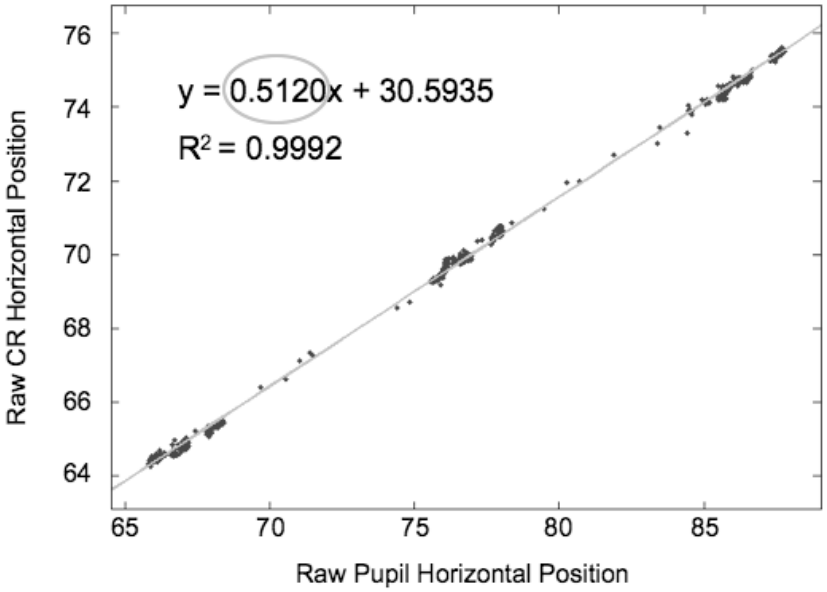

Figure 12: Linear regression for data shown in figure 11. The overlaid line is the calculated best-fit using least-squares regression and the slope (circled) of this line is equal to this observer's rotational gain.

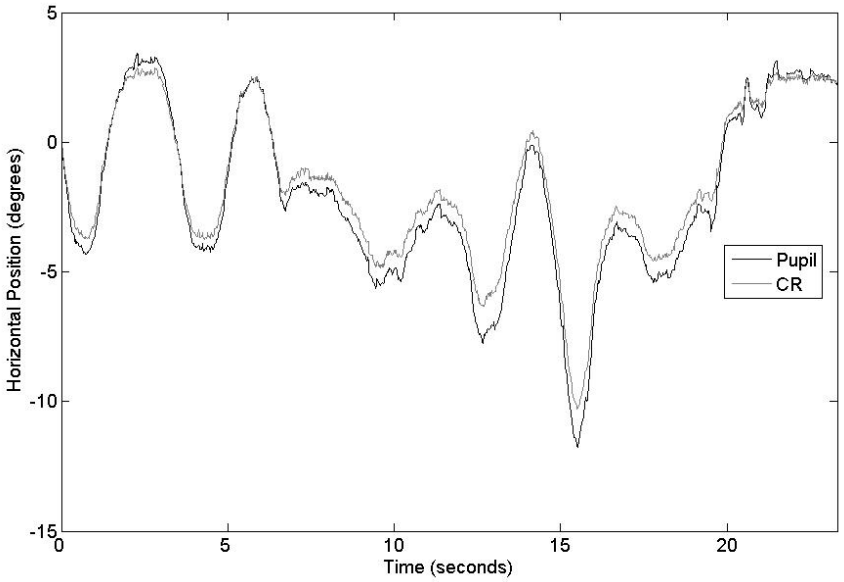

Figure 13: Example data from measuring the translational gain (observer 4).

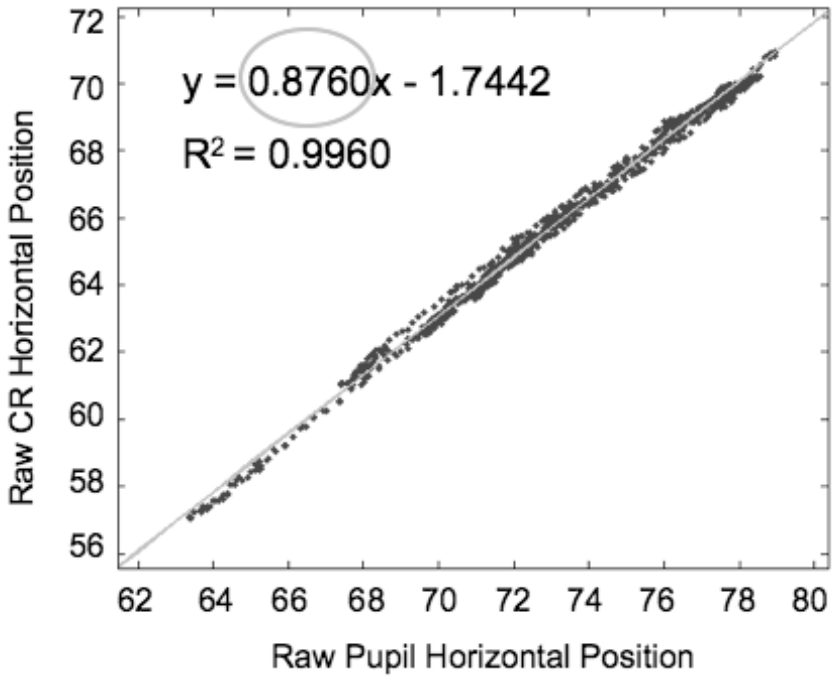

Figure 14: Linear regression for data shown in figure 13 from a camera movement trial. The overlaid line is the calculated best-fit using least-squares regression and the slope (circled) of this line is equal to this observer's translational gain.

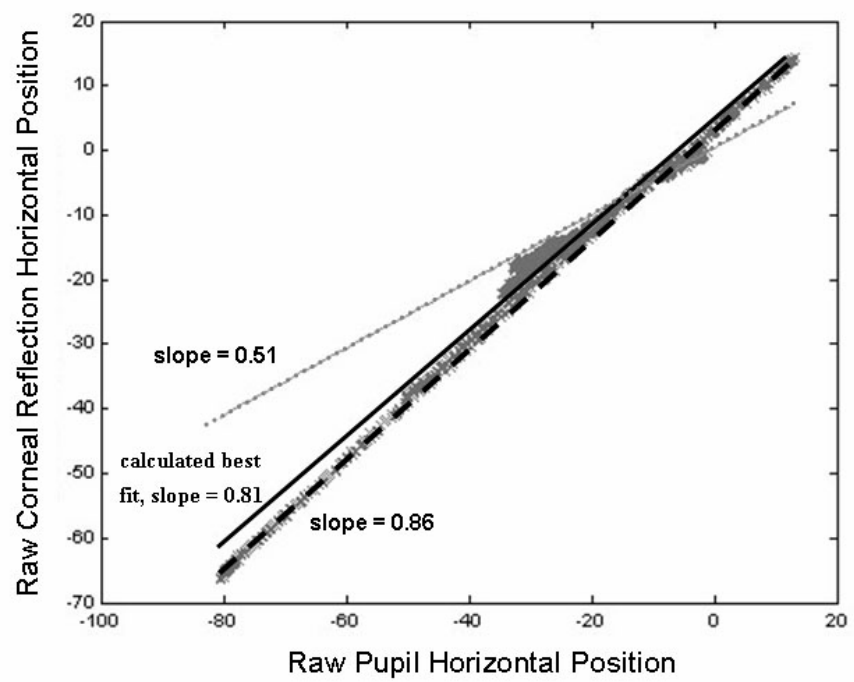

Figure 15: Data for observer 1 for measuring the translational gain shows the effect of possible coupling of rotational eye movements with translational eye movements (the latter due to camera movements). Using the average gain over five observers provides a better fit (dashed line) than that calculated for this observer (solid line). The subsection of data around a raw pupil position of -20 appears to fall along a line with slope equal to the average rotational gain of the five observers (dotted line).

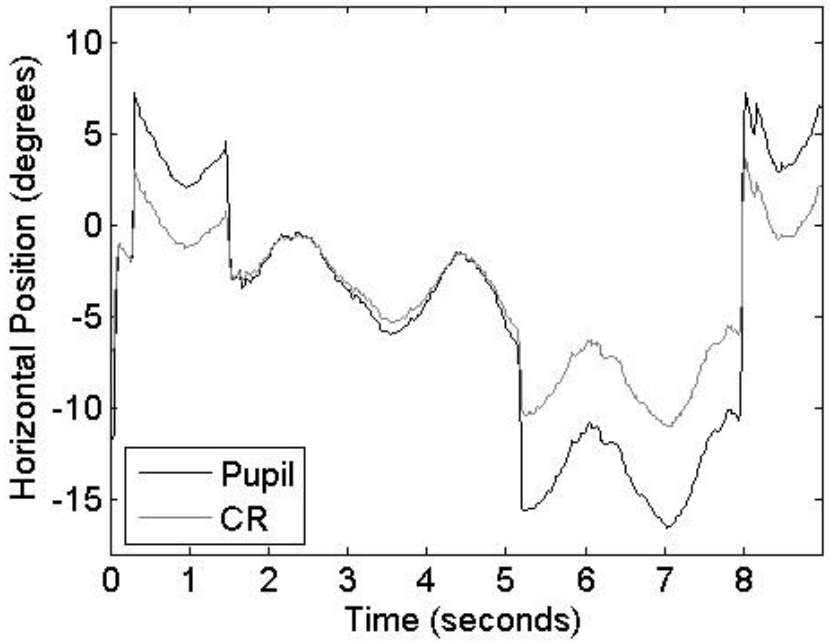

Figure 16: Pupil and CR data from observer 4 as he looked through the middle row of calibration points while moving the eye tracking headgear.

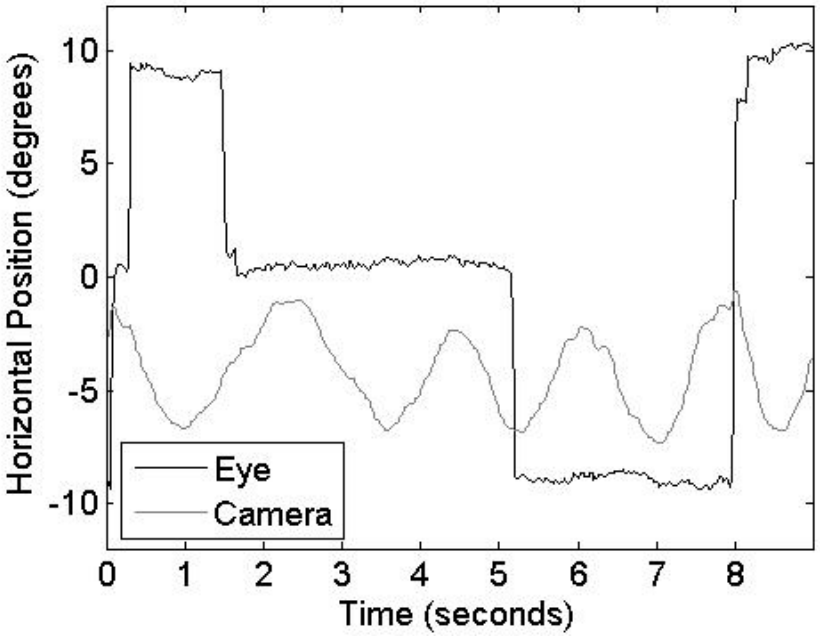

Figure 17: Eye and camera vectors from one observer during same segment shown in figure 16.

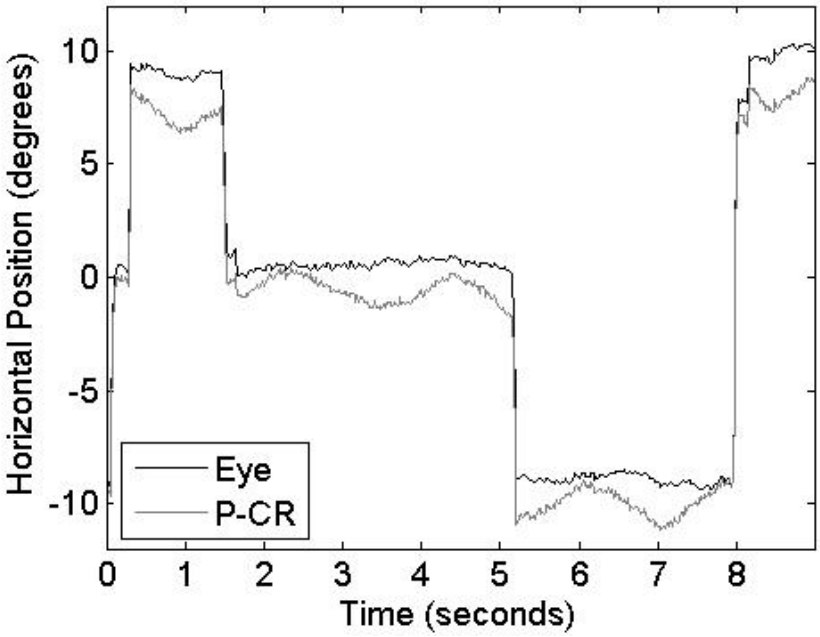

Figure 18: Eye vector compared to P-CR vector for same segment shown in previous two figures.

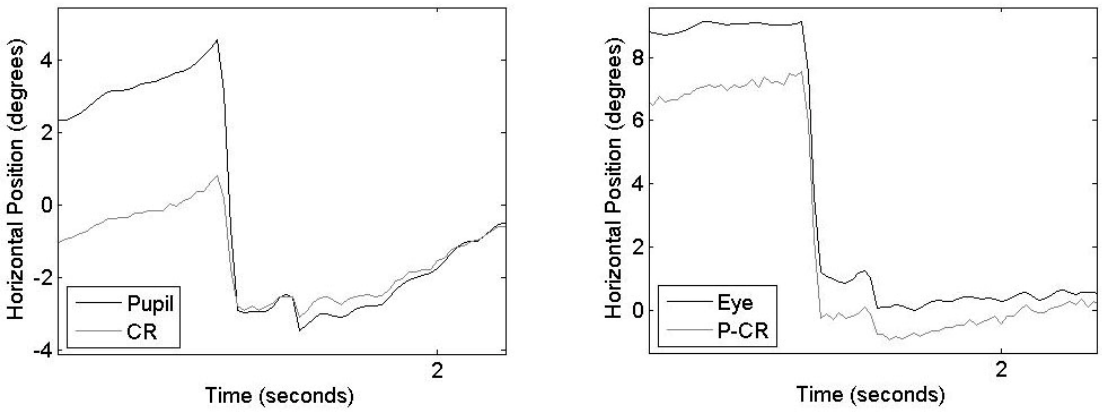

Figure 19: Zoomed-in view of horizontal position versus time from observer 4. (a) Pupil and CR position data; (b) Eye and P-CR data.

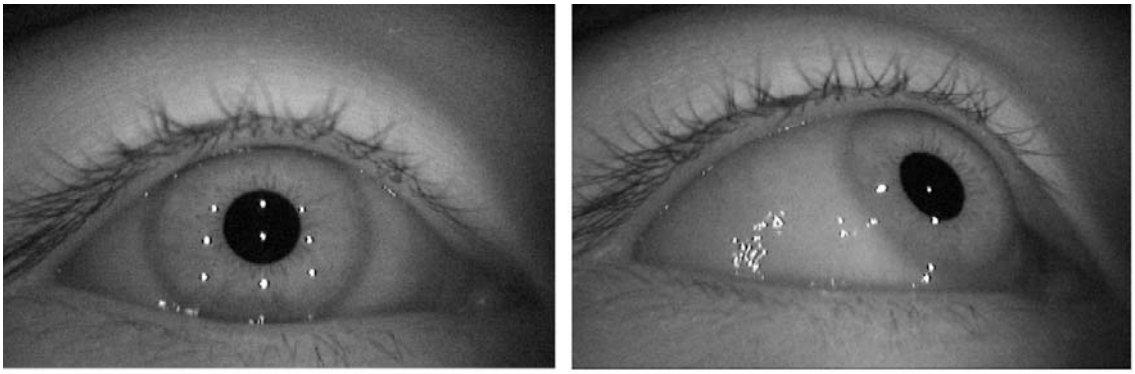

Figure 20. Eye images illuminated by the Structured Illumination scheme. (a) The eye looking straight ahead; (b) The eye moved to an extreme position.

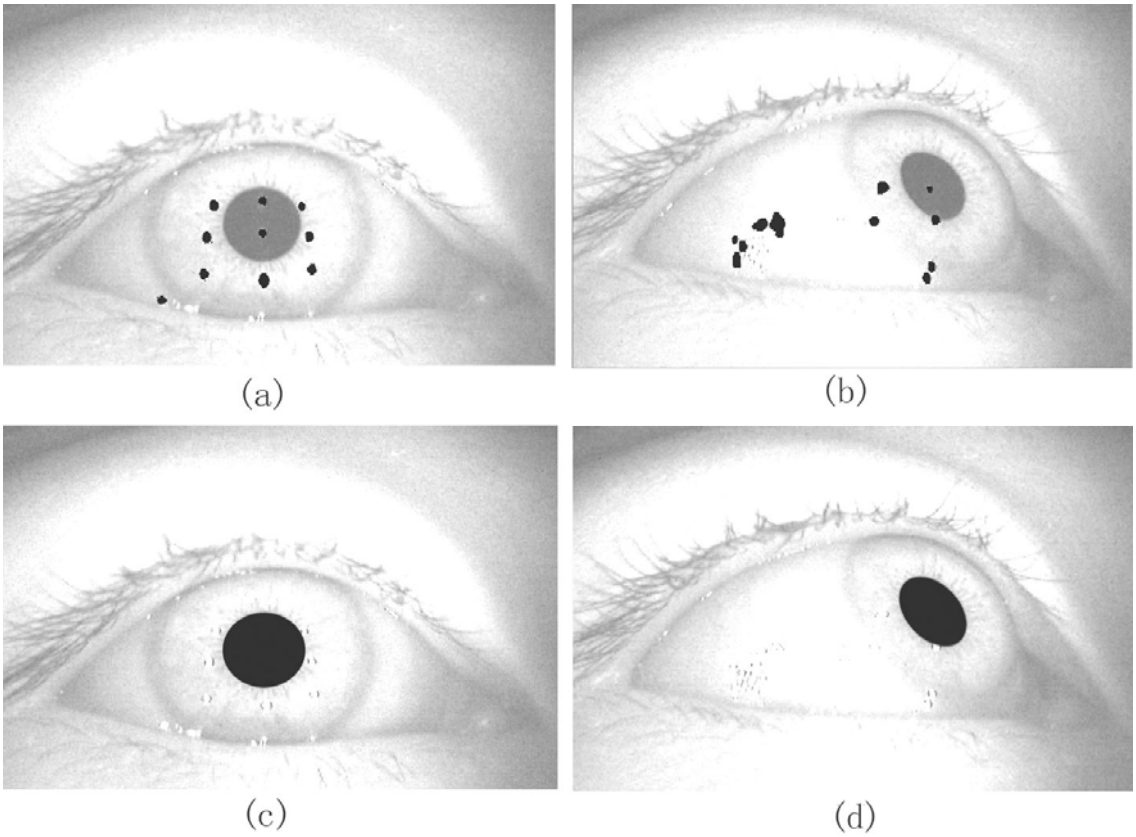

Figure 21: Processed eye images from figure 20: (a)(b) Potential CRs (black patches) after first-stage processing; (c)(d) Detected pupil areas (black elliptical areas). The background is brightened for display purposes.

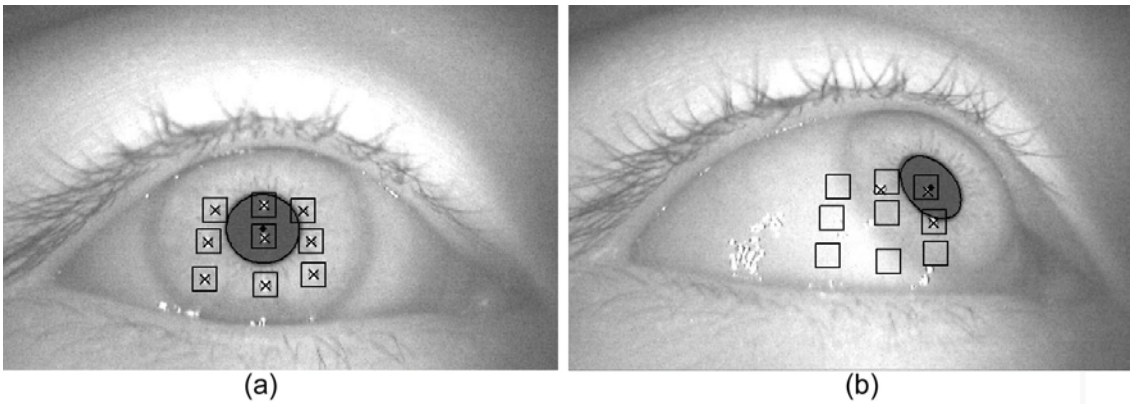

Figure 22: Desired CR discrimination utilizing the rotational gain on eye images in figure 20. Squares represent predicted CR regions, crosses represent detected desired CRs, ellipses represent the pupil boundary, and diamonds represent the pupil centroid. The background is brightened for display purposes.